Nonlinear Trajectory Tracking with a 6DOF AUV using an MRAFC Controller

Lugui Fenco, *Member, IEEE,* and Gustavo Pérez-Zuñiga *Member, IEEE*

***Abstract*—New technologies such as AUVs are used for marine exploration, considered a widespread solution in ocean monitoring, whose conventional controllers such as PID or LQR present inaccuracy in the path traversal and instability when faced with disturbances. Such that, in order to achieve sufficient precision in the path traversal and to be able to measure seabed parameters, the design of a Reference Model Adaptive Fuzzy Controller (MRAFC) is proposed. Which is a control strategy based on a combination of fuzzy systems theories using the Takagy-Sugeno model and adaptive control laws, respecting Lyapunov's nonlinear control theories to generate a robust control against inherent disturbances of the environment. Thus, the results obtained when comparing the MRAFC controller versus LQR and MRAC test controllers show better performance in different scenarios. Where the first scenario is ideal conditions, whose result is similar when the AUV is close to the origin and unstable in the LQR controller when it moves away from the design convergence point. A second scenario is considered the disturbances, obtaining unstable behaviors from the moment of the disturbance in the LQR and MRAC controllers, observing overstresses in the control variable τ causing chattering effect. While the last scenario is dedicated to recreate an environment with noise affecting the reading of the vehicle variables where only the MRAFC control law is able to compensate and control in a hostile environment. Therefore, based on the results of this research it is possible to identify the MRAFC controller as suitable for AUV where precision and stability are necessary.**

Link to graphical and video abstracts, and to code: https://latamt.ieeer9.org/index.php/transactions/article/view/9259

***Index Terms*—MRAFC, AUV, Lyapunov, Takagy-Sugeno, 6-DOF.**

I. Introduction

THE perception of climate change, pollution and the greenhouse effect has been increasing in recent years, experiencing significant variations in the temperature of several regions of the world, such as the record recorded in Greece in 2021 reaching 48.8 ° C [1]. While in the oceans it has generated variation in temperature, increased acidification, variation in salinity, etc., directly influencing health and causing the loss of the ecosystems that inhabit that environment. Taking as the most notable example the decrease in living coral reefs, which house countless coastal ecosystems, being one of the most productive on the planet, which has had a reduction of around 50% in the last 150 years [2], [3].

Motivated to investigate new technologies that allow exploring the seabed and traveling along defined trajectories, we find the Autonomous Underwater Vehicles (AUV), which are currently used for scientific exploration, oceanographic sampling, underwater archaeology, etc. [4], [5]. Where the objective is to collect data to be stored in the vehicle's internal memory or then transmitted to the surface to be analyzed and processed [6], [7].

However, the complex dynamics of the vehicle and the disturbances of the environment make it difficult to design a nonlinear controller with good performance [8], [9]. Therefore, our interest is focused on designing a controller for the AUV that allows exploring the coastal area of Peru, at depths not greater than 100 meters and that can follow trajectories specified by the user in order to monitor ocean parameters, generating the lowest tracking error. In addition, it must be robust to the dynamics of the environment, considering that it must generate a control law that adapts to time-dependent variables. Therefore, it is proposed to design a *Adaptive Fuzzy Controller by Reference Model* based on the Tagaki-Sugeno model and on the nonlinear control theories of Lyapunov to meet the design requirements.

Currently, conventional controllers are used for trajectory tracking, such as the IMC PID controller for AUV control, which is based on a split control scheme, with control subsystems for the *heading, dive plane and speed* loops. However, this type of control tends to be unstable under [10], [11] disturbances. In [12] we see a LQR multivariable controller, which through optimization manages to control the entire state vector of an Octocopter UAV. However, this type of control is effective near the equilibrium point. So, if the vehicle has more than one equilibrium point, it is necessary to opt for a hybrid controller such as LRQ-Fuzzy. Taking into account that such a scheme does not guarantee stability until the sufficient condition derived by Tanaka-Sugeno is met. In [13] we are shown a model-adaptive controller (MRAC) which converges on the reference signals, however overshoots and long settling times can be observed. We can also find some variants such as FUZZY-MRAC [14], with membership functions for the error and its derivative, presenting better performance, however it lacks a stability analysis. While in adaptive controllers that use NEURAL NETWORKS, trajectory tracking can be noted even when subjected to disturbances, but with long settling times in the state variable, generating steady-state error [15]. On the other hand, there are other more advanced control strategies such as SLIDING MODE controllers [16], [17], [18]

The associate editor coordinating the review of this manuscript and approving it for publication was Roberto S. Murphy (*Corresponding author: Lugui Fenco*).

Lugui Fenco, and G. Pérez-Zuñiga are with the Department of Engineering, Pontifical Catholic University of Peru, Lima, Perú (e-mails: paolo.fenco@pucp.edu.pe, and gustavo.perez@pucp.pe).

and DEEP REINFORCEMENT LEARNING controllers [19]. Thus, a quick inspection of the sliding mode controller shows good performance, however, a deeper analysis shows oscillations, characteristic of the chattering effect. When observing the dynamics of the deep reinforcement learning controller, it directly depends on capturing a large number of samples, which reduces the efficiency of the algorithm.

This article is structured as follows. Section II describes the static and dynamic equations of the nonlinear model, and presents the general vector equation of the AUV mentioning the main matrices of the dynamic equation. In section III, the linear model of the system for low speed applications is obtained assuming that the angles *phi* and *theta* are small, generating a new navigation system called "coordinate system parallel to the vehicle". In addition, the equations to obtain the equilibrium states of the nonlinear model are described. Section IV mentions the algorithm chosen for the generation of reference trajectories based on "Waypoint". Section V describes the design of LQR, MRAC test controllers, and the main controller of this MRAFC article. Briefly mentioning the lyapunov function used to obtain the equations of the adaptive law and describing the numerical optimization algorithm, LMIs, applied to the AUV model. Section VI shows the results obtained, performing a quantitative analysis using the ERMS performance index, obtaining comparative tables in different work scenarios described as *Ideal conditions, with disturbance and with noise*. Finally, section VII shows the conclusions.

II. Nonlinear Model of a 6DOF AUV

The nonlinear model of study for a 6DOF AUV is widely detailed in [20], [21], where a vectorial shape model according to Fossen can be obtained as:

$$\dot{\eta} = J_{\Theta}(\eta)\nu \tag{1}$$

$$\dot{\nu} = M^{-1}(-C(\nu)\nu - D(\nu)\nu - g(\eta) + \tau) \tag{2}$$

Where η is the position vector, while ν is the acceleration vector, and the union of these variables forms the state vector of the AUV. Also found are the inertial mass matrix M, the coriolis matrix C, the damping matrix D, the restoring force vector $g(\eta)$ and the propulsion force and moment vector τ.

The equation (1) corresponds to the *Kinematics* of the system, which deals with the geometric aspects of the motion and relates the body-fixed navigation frames $\{b\}$ and the NED frame $\{n\}$. In addition, the transformation matrix $J_{\Theta} = diag[R_b^n(\Theta_{nb}) \quad T_{\Theta}(\Theta_{nb})]$ is found, where $R_b^n(\Theta_{nb})$ and $T_{\Theta}(\Theta_{nb})$ are the linear and angular velocity transformation matrices respectively.

On the other hand, the equation (2) describes the *Dynamics* of the system, which performs an analysis of the forces that cause the movement. This can be divided into four different parts, such as: rigid body dynamics, hydrostatics, hydrodynamics and propulsion forces.

A. Rigid Body Dynamics

These equations arise due to the rotation of the reference frame $\{b\}$ about the reference frame $\{n\}$ and are expressed in vectorial form representing the rigid body dynamics as:

$$M_{RB}\dot{\nu} + C_{RB}(\nu)\nu = \tau_{RB} \tag{3}$$

Where M_{RB} represents the rigid body mass matrix, C_{RB} the rigid body coriolis and centripetal matrices and $\tau_{RB} = [X, Y, Z, K, M, N]$ is the vector of external forces and moments. Therefore, expanding this equation gives:

$$\begin{aligned} m[e - x_g(a) + y_g(pq - \dot{r}) + z_g(pr + \dot{q})] &= X \\ m[f - y_g(b) + z_g(qr - \dot{p}) + x_g(qp + \dot{r})] &= Y \\ m[d - z_g(c) + x_g(rp - \dot{q}) + y_g(rq + \dot{p})] &= Z \\ I_x\dot{p} + (I_z - I_y)qr + m[y_g(d) - z_g(f)] &= K \\ I_y\dot{q} + (I_x - I_z)rp + m[z_g(e) - x_g(d)] &= M \\ I_z\dot{r} + (I_y - I_x)pq + m[x_g(f) - y_g(e)] &= N \end{aligned} \tag{4}$$

Where $a = q^2+r^2$, $b = r^2+p^2$, $c = p^2+q^2$, $d = \dot{w}-uq+vp$, $e = \dot{u} - vr + wq$ and $f = \dot{v} - wp + ur$. In addition, one must take into account the vector $r_g = [x_g, y_g, z_g]$ which represents the vector from CO to CG.

B. Hydrostatics

The forces acting on the body of the vehicle are described as gravitational force and buoyancy force which are defined as: $W = mg, \quad B = \rho g \nabla$ [22], [23]

These forces act in the vertical plane of $\{n\}$ as f_g^n, f_b^n, so if these equations are to be expressed in the reference frame $\{b\}$ it is necessary to apply Euler transformations, thus obtaining $f_g^b = R_b^n(\Theta_n b)^{-1} f_g^n$ and $f_b^b = R_b^n(\Theta_n b)^{-1} f_b^n$. Considering F = W-B, then these equations can be expressed in vectorial form as:

$$g(\eta) = \begin{bmatrix} Fs\theta \\ -Fc\theta s\phi \\ -Fc\theta c\phi \\ -(y_g + y_b)F^T c\theta c\phi + (z_g + z_b)F^T c\theta s\phi \\ (z_g + z_b)F^T s\phi + (x_g + x_b)F^T c\theta c\phi \\ -(x_g + x_b)F^T c\theta s\phi - (y_g + y_b)F^T s\theta \end{bmatrix} \tag{5}$$

C. Hydrodynamics

The hydrodynamic effects for fluids such as ocean water are composed of elements such as the added mass matrix M_A and the damping matrix D, which are generated by the rotation of the navigation reference frame $\{s\}$ and the inertial reference frame $\{n\}$. Therefore, to understand the dynamics of these components, each of them will be briefly described below.

Added mass: This matrix represents the counterforce to the AUV's motion when it is submerged, and is proportional to the vehicle's acceleration. Therefore, this matrix is defined as:

$$\begin{aligned} -X_{\dot{u}} - a_{12} + a_{13} &= X_{add} \\ -Y_{\dot{v}} - Y_{\dot{r}} + a_{12} - a_{23} &= Y_{add} \\ -Z_{\dot{w}} - Z_{\dot{q}} - a_{13} + a_{23} &= Z_{add} \\ -K_{\dot{p}} - a_{12} + a_{13} - b_{12} + b_{13} &= K_{add} \\ -M_{\dot{w}} - M_{\dot{q}} + a_{12} - a_{23} + b_{12} - b_{23} &= M_{add} \\ -N_{\dot{v}} - N_{\dot{r}} - a_{13} + a_{23} - b_{13} + b_{23} &= N_{add} \end{aligned} \tag{6}$$

Where: $a_{12} = (Z_{\dot{w}}w + Z_{\dot{q}}q)$, $a_{13} = (Y_{\dot{v}}v + Y_{\dot{r}}r)$, $a_{23} = X_{\dot{u}}u$, $b_{12} = (N_{\dot{v}}v + N_{\dot{r}}r)$, $b_{13} = (M_{\dot{w}}w + M_{\dot{q}}q)$ and $b_{23} = K_{\dot{p}}p$.

hydrodynamic damping: The motion of the AUV underwater generates a friction due to the viscosity of the fluid. Such a viscous force is defined as $F_v = \frac{1}{2}\rho\nu^2 AC_D$. Where ρ is the density of the fluid, ν is the velocity of the AUV, A the area projected onto an orthogonal plane and C_D the drag coefficient. Therefore, according to Fossen [2], this matrix is defined as:

$$D = \begin{bmatrix} X_D & 0 & 0 & 0 & 0 & 0 \\ 0 & Y_D & 0 & 0 & 0 & 0 \\ 0 & 0 & Z_D & 0 & 0 & 0 \\ 0 & 0 & 0 & K_D & 0 & 0 \\ 0 & 0 & M_D w & 0 & M_D q & 0 \\ 0 & N_D v & 0 & 0 & 0 & N_D r \end{bmatrix} \tag{7}$$

Where: $X_D = X_{u|u|}u|u|$, $Y_D = Y_{v|v|}v|v|$, $Z_D = Z_{w|w|}w|w|$, $K_D = K_{p|p|}p|p|$, $M_D q = M_{q|q|}q|q|$,$M_D w = M_{w|w|}w|w|$,$N_D r = N_{r|r|}r|r|$,$N_D v = N_{v|v|}v|v|$.

D. Forces and Moments of Propulsion

These forces act on the AUV and are located in such a way that each thruster will depend on the geometry of the vehicle, so that symmetry helps reduce the complexity of the calculation by canceling moments. Therefore, it was decided to establish main thrust forces defined as Tport; Tstbd, which offer movement along the X axis. Then, thrust forces defined as Tforeh; Tafth; Tforev and Taftv were established, which act as stabilizers along the Y and Z axes.

$$\tau = \begin{bmatrix} 1 & 1 & 0 & 0 & 0 & 0 \\ 0 & 0 & 1 & 1 & 0 & 0 \\ 0 & 0 & 0 & 0 & 1 & 1 \\ z_p & z_p & x_{pf} & -x_{pa} & -x_{pf} & x_{pa} \\ z_p & z_p & 0 & 0 & -x_{pf} & x_{pa} \\ y_p & -y_p & x_{pf} & -x_{pa} & 0 & 0 \end{bmatrix} \begin{bmatrix} T_{port} \\ T_{stbd} \\ T_{fore_h} \\ T_{aft_h} \\ T_{fore_v} \\ T_{aft_v} \end{bmatrix} \tag{8}$$

III. Linear Model of a 6DOF AUV

The nonlinear model obtained in the previous section has sufficient complexity to capture the dynamic characteristics of the AUV. Therefore, designing a controller for this system has a very high degree of difficulty because most of the terms present in the equations are nonlinear, such as the trigonometric terms of sines and cosines in equations (1) and (2). Therefore, to address this problem, it is chosen to make a linear model based on the nonlinear model to design a controller.

To design the linear system it will be assumed that the angles ϕ, θ *are small* ($\phi, \theta \approx 0$) where the movements in the angles *roll* and *pitch* are limited, i.e. highly stable. This type of approximation converts the transformation matrix $J_\Theta(\eta)$ into a reduced form called matrix $P(\psi)$.

$$\dot{\eta} = J_\Theta(\eta)\nu \overset{\phi=\theta=0}{\approx} P(\psi)\nu \tag{9}$$

donde

$$P_\psi := \begin{bmatrix} R(\psi) & I_{3x3} \\ I_{3x3} & I_{3x3} \end{bmatrix} \tag{10}$$

and $R(\psi) = R_{z,\psi}$ is the rotation matrix in *yaw*.

Now, due to the assumption that $\phi, \theta \approx 0$, a new coordinate system called *Vehicle Parallel (VP) Coordinate System* can be established defined as $\eta_p = P^T(\psi)\eta$. Where η_p is the NED position and location vector expressed in $\{b\}$ and $P(\psi)$ is given by the equation (10). Considering that $P^T(\psi)P(\psi) = I_{6x6}$

A. Low Speed Applications

It is convenient to express the kinematics equations in VP coordinates when using linear theory. Therefore, deriving η_p gives:

$$\dot{\eta}_p = rS\eta_p + \nu \tag{11}$$

where $r = \dot{\psi}$ and $S \in R_{6x6}$ is a constant matrix. Then, for low speed applications ($r \approx 0$), the equation (11) can be reduced to six pure integrators.

$$\dot{\eta}_p \approx \nu \tag{12}$$

So this model is useful because it is now linear in ν. In fact, that is the main idea for using VP coordinates in control designs on ships and platforms.

On the other hand, the gravitational force and the buoyant force can also be expressed in terms of the VP coordinate system, resulting in:

$$g(\eta) \overset{\phi=\theta=0}{\approx} \underbrace{P^T(\psi)GP(\psi)\eta_p}_{G} = G\eta_p \tag{13}$$

Where G is defined as:

$$G = diag[0, 0, 0, (z_g W - z_b B), (z_g W - z_b B), 0] \tag{14}$$

Thus, the result in equation (13) confirms that the restoring forces of a level vehicle are independent of the *yaw* angle ψ. Furthermore, for low speed applications ($v \approx 0$) it implies that the forces and moments in equation (2) can be linearized as $C(\nu) = C(0) = 0$ and $D(\nu) = D\nu$. Then it makes sense to approximate:

$$M\dot{\nu} + \underbrace{\cancel{C(\nu)}\nu}_{0} + \underbrace{[D + \cancel{D_n(\nu)}]\nu}_{D\nu} + \underbrace{g\eta}_{G\eta_p} = \tau_{total} \tag{15}$$

Where $D_n(\nu)$ is the nonlinear damping matrix due to quadratic and higher order terms, and $\tau_{total} = \tau + \underbrace{\tau_{wind} + \tau_{wave}}_{w}$. Then the following equations expressed in PV are obtained:

$$\begin{aligned} \dot{\eta}_p &= \nu \\ M\dot{\nu} + D\nu + G\eta_p &= \tau + w \end{aligned} \tag{16}$$

This is the linear and time-invariant state-space model.

$$\dot{x} = Ax + Bu + Ew \tag{17}$$

where $x = [\eta_p^T, \nu^T]^T$, $u = \tau$ and

$$A = \begin{bmatrix} 0 & I \\ -M^{-1}G & -M^{-1}D \end{bmatrix}, \quad B = \begin{bmatrix} 0 \\ M^{-1} \end{bmatrix}, \quad E = \begin{bmatrix} 0 \\ M^{-1} \end{bmatrix} \tag{18}$$

Considering that the NED positions are calculated from η_p using:

$$\eta = P(\psi)\eta_p \tag{19}$$

Therefore, the control system can be based on feedback from the states $(\eta_p,\ \nu)$ while η is presented to be the human operator in use.

B. States of Convergence

A linear model is obtained from a convergence state, which can be local or global and is obtained from the non-linear model. Therefore, from the equation (1) and (2) we can obtain the convergence states of the AUV:

$$\begin{aligned} \dot{\eta}^* &= J_\Theta(\eta^*)v^* \\ \dot{v}^* &= M^{-1}(-C(v^*)v^* - D(v^*)v^* - g(\eta^*) + \tau^*) \end{aligned} \tag{20}$$

Where $\dot{\eta}^* = 0, \dot{v}^* = 0$ must be satisfied. Then, considering that for low speed applications $\nu^* \approx 0$ and that the system is neutral in buoyancy $W = B$, $g(\eta^*)$ can be reduced to:

$$g(\eta) = \quad - \begin{bmatrix} 0 \\ 0 \\ 0 \\ (z_g W - z_b B)\cos(\theta)\sin(\phi) \\ (z_g W - z_b B)\sin(\theta) \\ 0 \end{bmatrix} \tag{21}$$

Furthermore, the matrices $C(\nu)$,$D(\nu)$ can be simplified by considering again that the AUV will have a displacement parallel to the coordinate system (VP), thus obtaining an approximation of $g(\eta^*) \approx G\eta^*$. Likewise, it must also be considered that $\tau^* = 0$. Therefore, neglecting the elements that must be cancelled in the equations of the system, we obtain:

$$\begin{aligned} 0 &= J_\Theta(\eta^*)v^* \\ 0 &= M^{-1}(-\cancel{C(\theta)v^*} - \cancel{D(\theta)v^*} - G\eta^* + \cancel{\tau^*}) \end{aligned} \tag{22}$$

Expanding the above equations, we can obtain four main equations, while in any other case it is zero:

$$\begin{aligned} 0 &= u^*\cos(\psi^*) - v^*\sin(\psi^*) \\ 0 &= u^*\sin(\psi^*) + v^*\cos(\psi^*) \\ 0 &= \left(\frac{1}{I_{xx} - K_{\dot{p}}}\right)[-(z_G W - z_b B)\phi^*] \\ 0 &= \left(\frac{1}{I_{yy} - K_{\dot{q}}}\right)[-(z_G W - z_b B)\theta^*] \end{aligned} \tag{23}$$

Therefore, after performing simple algebraic calculations, we can obtain the following points of convergence:

$$\begin{aligned} [\eta^*, \nu^*] &= [x^*, y^*, z^*, 0, 0, 0, 0, 0, 0, 0, 0, 0]^T \\ [\eta^*, \nu^*] &= [x^*, y^*, z^*, 0, 0, \pi/2, 0, 0, 0, 0, 0, 0]^T \\ [\eta^*, \nu^*] &= [x^*, y^*, z^*, 0, 0, -\pi/2, 0, 0, 0, 0, 0, 0]^T \\ [\eta^*, \nu^*] &= [x^*, y^*, z^*, 0, 0, \pi, 0, 0, 0, 0, 0, 0]^T \end{aligned} \tag{24}$$

IV. Controller Design

From the convergence states obtained in section IV, we can establish a linear subsystem in each of them. Furthermore, considering that there are parameters that change over time, such as the case of hydrodynamic parameters, the design must require a control strategy that can switch between the different convergence states in a smooth manner, while on the other hand there is the need for it to be able to adapt to the time-dependent variables, in order to asymptotically travel the desired trajectory and at the same time be a robust design against disturbances and noise. Therefore, it was chosen to design a model-adaptive fuzzy controller (MRAFC) capable of meeting the aforementioned requirements. In this section, the final equations of the MRAFC controller will be mentioned because it is widely developed in [24], [25]. In order to compare the performance of the MRAFC controller, additional controllers were designed such as the linear quadratic regulator (LQR) and the model-adaptive controller (MARC).

A. LQR Controller

This controller is derived from the optimal control theory, which is based on obtaining a control law such that the following cost function is minimized:

$$J = \int_0^\infty (x^T Q x + u^T R u) \tag{25}$$

Where Q and R are weight matrices associated with each of the input and output variables in the equation (25).

Therefore, for the design the linearized system obtained in section IV is used such that:

$$\dot{\hat{x}} = A\hat{x} + B\hat{u}, \quad \hat{u} = -K\hat{x} \tag{26}$$

Where K is the controller gain matrix, $\hat{x}$ is defined as $(x - x^*)$ whose vector x^* is the convergence vector of the system state vector x and $\hat{u}$ is defined as $(u - u^*)$ where u^* is the convergence vector of the input vector u.

B. MRAC Controller

The MRAC controller chooses the control law such that the closed-loop plant transfer function is equal to the reference model, ensuring that the plant output y_p follows the model output y_m and that the error tends to zero. Next, a matching law is chosen based on a feedback only to the plant, using an offset defined by the transfer function matrix R_p:

$$\begin{aligned} \dot{s_p}(t) &= A_s s_p(t) + B_s u_p(t) \\ r_p(t) &= D_s s_p(t) \end{aligned} \tag{27}$$

The increased output to control then is:

$$z_p(t) = y_p(t) + r_p(t) \tag{28}$$

The augmented system is:

$$G_a(s) = G_p(s) + R_p(s) \tag{29}$$

where $G_a(s)$ is ASPR whenever:

- $R_p(s)$ is such that the relative degree of $G_a(s)$ is m.

- $R_p^{-1}(s)$ stabilizes the closed-loop output feedback system with the transfer function $[I + G_p(s)R_p^{-1}(s)]^{-1}G_p(s)$.

By sizing the plant with a feedforward compensator $R_p(s)$, which satisfies the above conditions, and having a minimum a priori knowledge, a stability configuration can be designed. That is, if a plant is stabilized by a PD controller $R_p^{-1}(s) = K(1 + \frac{s}{s_o})$, all that is needed is the estimate of the highest gain $K = K_{max}$ that maintains stability. Such that:

$$R_p(s) = \frac{K_{max}^{-1}}{\frac{s}{s_o}} \tag{30}$$

For any general stabilization configuration, it is important to find the highest gain that maintains stability. That way, $R_p^{-1}(s)$ has a small gain, and the output $r_p(t)$ will remain small relative to the plant output $y_p(t)$. Through the addition of $R_p(s)$ one can improve the stabilization properties of the adaptive system, so it is desired that the increased output $z_p(t)$ remain approximately equal to the plant output $y_p(t)$.

C. MRAFC Controller

Considering that some plant parameters are unknown and the objective of the design is to formulate a control law, as well as an adaptation law for the time-varying parameters, so that the plant output follows the reference signal ensuring stability, it will be necessary to use mathematical tools such as Lyapunov theories and apply the Takagi-Sugeno model.

1) Takagi-Sugeno model: This model is described by fuzzy IF-THEN rules as:

$$\begin{aligned} R^i: \quad & \text{If } x_1(t) \text{ is } M_1^i \text{ and} \dots \text{ and } x_n(t) \text{ is } M_n^i \\ & \text{then} \quad x(t) = A_i x(t) + B_i u(t) \\ & \qquad\quad u(t) = -K_i\ x(t) \end{aligned} \tag{31}$$

Where the vector $x^T(t) = [x_1(t), x_2(t), \dots, x_n(t)]$ and the vector $u^T(t) = [u_1(t), u_2(t), \dots, u_n(t)]$. Now given a pair of inputs $(x(t), u(t))$, the closed-loop fuzzy control system can be constructed as:

$$\dot{x}(t) = \frac{\sum_{i=1}^{l}\sum_{j=1}^{l} w_i(t)\ w_j(t)\{A_i - B_i\ K_j\}x(t)}{\sum_{i=1}^{l}\sum_{j=1}^{l} w_i(t)w_j\ (t)} \tag{32}$$

Where $w_i(t) = \prod_{j=1}^{n} M_j^i(x_j(t))$, and $M_j^i(x_j(t))$ is the membership degree of $x_j(t)$ in M_j^i.

While, in a similar process a T-S model can be established for the reference model defined as:

$$\dot{x}_m = \frac{\sum_{i=1}^{l}\sum_{j=1}^{l} w_i(x)\ \mu_j(x)\{(A_m)_{ij}\ x_m + (B_m)_{ij}\ r\}}{\sum_{i=1}^{l}\sum_{j=1}^{l} w_i(x)\ \mu_j\ (x)} \tag{33}$$

Where $x \in R^n$ is the state vector, $A_i \in R^{nxn}$, $B_i \in R^{nxq}$ (i) $(i = 1, 2, \dots, l)$ are known matrices and (A_i, B_i) are controllable. The control objective is to choose an input vector $u \in R^q$ such that x follows x_m of the reference model.

Considering that the matrices A_i, B_i are known, therefore, it is possible to propose the following control law:

$$u = \sum_{j=1}^{l} \mu_j(x)(-K_j(t)\ x + L_j(t)\ r) / \sum_{i=1}^{l} \mu_j(x) \tag{34}$$

So, for the control law (34) to satisfy the control objective it is necessary that the matrices K_j and L_j have sufficient structural flexibility.

2) Adaptive Law: In order to derive the adaptive law, the equations of the nonlinear model and the reference model must first be expressed in terms of the tracking error, which is defined as $e \cong x - x_m$ and taking into account the identity $B_i = (B_m)_{ij}L_j^{*-1}$, we obtain:

$$\begin{aligned} \dot{e} = & \frac{\sum_{i=1}^{l}\sum_{j=1}^{l} w_i(x)\ \mu_j(x)(A_m)_{ij}}{\sum_{i=1}^{l}\sum_{j=1}^{l} w_i(x)\ \mu_j(x)} e \\ & + \frac{\sum_{i=1}^{l}\sum_{j=1}^{l} w_i(x)\ \mu_j(x)(B_m)_{ij}L_j^{*-1}(-\widetilde{K}_j\ x + \widetilde{L}_j\ r)}{\sum_{i=1}^{l}\sum_{j=1}^{l} w_i(x)\ \mu_j(x)} \end{aligned} \tag{35}$$

Where $\widetilde{K_j} = K_j(t) - K_j^*$ and $\widetilde{L_j} = L_j(t) - L_j^*$. Then, we can assume that L_j^* can be a positive definite or negative definite matrix. Such that, it is possible to define $\Gamma_j^{-1} = L_j^* sgn(l_j)$, where $l_j = -1$ if L_j^* is negative definite. Then an adaptive law is derived to update the control parameters K_j^*, L_j^*. Therefore, the following candidate Lyapunov function is proposed:

$$V(e, \widetilde{K_j}, \widetilde{L_j}) = e^T P e + \sum_{i=1}^{l} tr(\widetilde{K}_j^T \Gamma_j \widetilde{K}_j + \widetilde{L}_j^T \Gamma_j \widetilde{L}_j) \tag{36}$$

Where $P = P^T > 0$ is a common positive definite matrix of the Lyapunov equation $(A_m)_{ij}^T P + P(A_m)_{ij} < -Q_{ij}$ for all $Q_{ij} = Q_{ij}^T > 0$ $(i = 1, \dots, l)$ whose existence is a guarantee to assume the stability of A_m. Therefore, the obvious choice of an adaptive law that makes $\dot{V}$ negative is:

$$\dot{\widetilde{K}}_j = \dot{K}_j(t) = \frac{\sum_{i=1}^{l}\sum_{j=1}^{l} w_i(x)\mu_j(x)(B_m)_{ij}^T sgn(l_j)}{\sum_{i=1}^{l}\sum_{j=1}^{l} w_i(x)\mu_j(x)} P e x^T \tag{37}$$

$$\dot{\widetilde{L}}_j = \dot{L}_j(t) = -\frac{\sum_{i=1}^{l}\sum_{j=1}^{l} w_i(x)\mu_j(x)(B_m)_{ij}^T sgn(l_j)}{\sum_{i=1}^{l}\sum_{j=1}^{l} w_i(x)\mu_j(x)} P e r^T \tag{38}$$

3) Linear matrix inequality: A fundamental part of the MRAFC controller design is to be able to compute the positive definite matrix P in equations (37) and (38). Therefore, this problem becomes finding a matrix such that it satisfies the Lyapunov stability condition on all linear subsystems of the AUV. This then becomes developing numerical optimization problems also known as LMIs problems, whose most efficient development method is the interior point method. Such that, we can define a linear matrix inequality (LMIs) as:

$$F(x) = F_0 + \sum_{i=1}^{m} x_i F_i > 0 \tag{39}$$

Where $x^T = (x_1, x_2, \ldots, x_m)$ is the variable to be determined and the symmetric matrices $F_i = F_i^T \in \mathbb{R}^{nxn}, 0 \leq i \leq m$. The inequality symbol given in equation (39) means that $F(x)$ is positive definite, that is, $v^T F(x) v < 0$ for all $v \in \mathbb{R}^n$ nonzero. The equation (39) is a convex restriction on x, that is, the set $\{x \mid F(x) > 0\}$ is convex.

Now considering the following closed-loop linear system:

$$\dot{x} = Ax + Bu, \quad u \ = -Fx \tag{40}$$

Where $B_i \in \mathbb{R}^{nxm}$, $u \in \mathbb{R}^m$ and the feedback gain $F \in \mathbb{R}^{mxn}$. Then, we can make use of the stability condition for continuous time systems which is given by:

$$A^T P - F^T B^T P + PA - PBF < 0, \qquad P > 0 \tag{41}$$

As shown, the above inequality is not considered an LMI condition for matrices P and F. In order for it to be converted to an LMI condition, it must be multiplied on both sides by $X = P^{-1}$ and establish that $M = FX$, with which this inequality becomes:

$$XA^T - M^T B^T + AX - BM < 0, \qquad X > 0 \tag{42}$$

Hence, the inequality (42) becomes an LMI condition for matrices X and M. Matrices P and F can be computed from $P = X^{-1}$ and $F = MX^{-1}$, where X^{-1} represents the inverse of X. Then the following LMIs can be obtained:

$$\begin{gathered} -XA_i^T - A_i X + M_i^T B_i^T + B_i M_i < 0 \\ -XA_i^T - A_i X - XA_j^T - A_j X + M_j^T B_i^T + B_i M_j \\ +M_i^T B_j^T + B_j M_i < 0 \end{gathered} \tag{43}$$

V. Simulation Results

Now, focused on testing the nonlinear model of the 6DOF AUV obtained in section III, our objective will be to apply the MRAFC control law developed in section V and compare the results obtained with the LQR and MRAC test controllers. Therefore, in order to do this, it is necessary to develop a simulation of the dynamic behavior of both the nonlinear system and the MRAFC controller using MATLAB software.

This simulation is composed of two sections. The first section is dedicated to the analysis of the dynamic behavior of the AUV in the regulation stage, establishing certain values in the state vector η, until reaching convergence and stability at these desired values. While the next section will show results regarding the tracking stage, dedicated to trajectory tracking.

Algorithm 1 LMI conditions algorithm

1: The non-linear system of an AUV is considered in vector form as:
$\dot{\eta} = J_\Theta(\eta) v$
$M\dot{v} + C(v)v + D(v)v + g(\eta) + g_0 = \tau + \tau_{wind} + \tau_{wave}$
2: The convergence points of the nonlinear system are obtained $\eta \to \eta^*, \nu \to \nu^*, \tau \to \tau^*$, Considering that $\dot{\eta}^* \to 0, \dot{\nu}^* \to 0$. Therefore, the system takes the following form:
$0 = J_\Theta(\eta^*) v^*$
$0 = M^{-1}(-C(v^*)v^* - D(v^*)v^* - g(\eta^*) + \tau^*)$
3: Then, the Takagi-Sugeno linear model is obtained for each of the convergence points previously obtained:
$\sum x(t) = A_i x(t) + B_i u(t)$
4: To ensure the stability of the linear system, the following conditions must be met:
$A^T P - F^T B^T P + PA - PBF < 0, \qquad P > 0$
5: However, it is not considered an LMI condition, so a conversion must be done using:
$X = P^{-1}$ and $M = FX$
6: with which this inequality becomes:
$XA^T - M^T B^T + AX - BM < 0, \qquad X > 0$
7: To develop the previous inequality, the variables will be defined with the following dimensions:
$Q \leftarrow lmivar(size(A1, 1))$
$M1, M2, M3, M4 \leftarrow lmivar(size[6\ 12])$
8: The LMI can be divided into three groups of inequalities.The first group is made up of matrices A and B of each point of convergence and which will be evaluated with variables Q and M.
$A_1 X + XA_1^T + B_1 M_1 + M_1^T B_1^T \leftarrow lmiterm(Q, A1, M1, B1)$
$A_2 X + XA_2^T + B_2 M_2 + M_2^T B_2^T \leftarrow lmiterm(Q, A2, M2, B2)$
$A_3 X + XA_3^T + B_3 M_3 + M_3^T B_3^T \leftarrow lmiterm(Q, A3, M3, B3)$
$A_4 X + XA_4^T + B_1 3 M_4 + M_4^T B_4^T \leftarrow lmiterm(Q, A4, M4, B4)$
9: The second group is made up of the combination of matrices A and B of convergence points 1 - 2, which will be evaluated with the variables M1, M2 and Q.
$A_1 X + XA_1^T + A_2 X + XA_2^T \leftarrow lmiterm(Q, A1, A2)$
$B_1 M_2 + M_2^T B_1^T + B_2 M_1 + M_1^T B_2^T \leftarrow lmiterm(M2, M2, B1, B2)$
10: The third group is made up of the combination of matrices A and B of convergence points 3 - 4, which will be evaluated with the variables M3, M4 and Q.
$A_3 X + XA_3^T + A_4 X + XA_4^T \leftarrow lmiterm(Q, A3, A4)$
$B_3 M_4 + M_4^T B_3^T + B_4 M_3 + M_3^T B_4^T \leftarrow lmiterm(M3, M4, B3, B4)$
11: Then, a solution is obtained for x^{feas}
$[tmin, xfeas] \leftarrow feasp(lmisys)$
12: Get value of Q, M_i
$Qopt, Mopt_i \leftarrow dec2mat(xfeas, Q, M_i)$
13: Finally, calculate the matrix P y F_i
$P \leftarrow inv(Qopt)$; $F_i \leftarrow Mopt_i * P$

A. Regulation

For this regulation stage, we evaluate the convergence of the state vector η and the output vector u at three given values. Where, the following values have been chosen:

- $\eta_1 = [x_1, y_1, z_1, \phi_1, \theta_1, \psi_1] = [2, -2, 1, 0^o, 0^o, 180^o]$.
- $\eta_2 = [x_2, y_2, z_2, \phi_2, \theta_2, \psi_2] = [1.2, -1.2, 2, 0^o, 0^o, 180^o]$.
- $\eta_3 = [x_3, y_3, z_3, \phi_3, \theta_3, \psi_3] = [0.6, 0.8, 3, 0^o, 0^o, 110^o]$.

These values have been chosen in such a way that in the first two items η_1 and η_2 the controllers LQR, MRAC and MRAFC are within their usual working range or as close to their equilibrium state as possible, so it is expected that all of them control and converge the system at the proposed

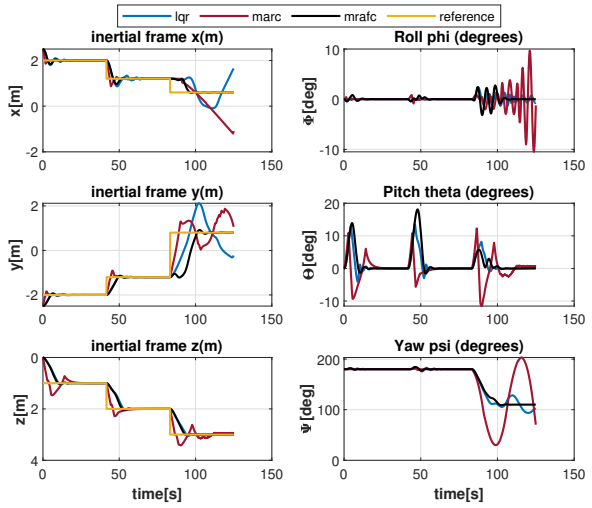

Fig. 1. Time response of the state vector η in the regulation stage, showing the dynamics of the AUV when convergence values η_1, η_2, η_3 move away from the equilibrium state of the origin.

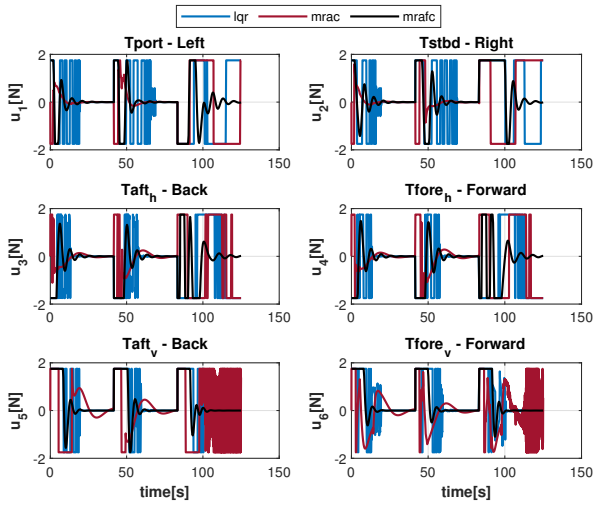

Fig. 2. Time response of the output vector u in the regulation stage, showing the behavior of the thrusters at each of the convergence values η_1, η_2, η_3.

values. While the last item η_3 was determined to be far from its equilibrium state.

The left side of Fig. 1 shows the time response of the position vector where we can observe that the AUV converges correctly in the time range $t = [0, 84]$. While in the remaining time, the inestability starts for the LQR and MRAC controllers, while MRAFC maintains the convergence at the desired value.

Considering the initial position of the AUV at $\eta_0 = [2.5, -2.5, 0, 0^o, 0^o, 180^o]$, we have an average settling time in the interval $t = [0, 42]$ of 14s with respect to the variable x, 20s for the variable y and 30s for the variable z. Then, in the interval, $t = [42, 84]$, a time of 20s for x, 20s for y and 35s for z is observed. While in the remaining time, only one controller converges, MRAFC, with values of 15s for x, 20s for y and 12s for z. Where we can notice that the higher the step height, the longer the settling time.

Another feature to notice is the undershoot, with a higher value in the variable z of the MARC controller, reaching around 90% of the step signal height in the interval $t = [0, 42]$, while in the interval $t = [42, 84]$ it manages to reach 75% of the step height. On the other hand, the responses of the LQR and MRAFC controllers show a lower value, highlighting the MRAFC controller, which reaches on average 20% in x, 3% in y and 3% in z.

Next on the right side of Fig. 1 is the orientation vector, where we can observe in the interval $t = [0, 84]$ that the variable *pitch* of the MRAFC controller has peaks of 18^o, being higher than LQR and MRAC. This is due to the stepped descent and the rapid action of the controller to stabilize the system producing high peaks. While, in the interval $t = [84, 125]$ it shows a sinusoidal instability in the variables *roll* and *Yaw* in MRAC, but with convergence in LQR and MRAFC. The only variable that converges in the three controllers is the variable *pitch*.

Then, in Fig. 2 the output vector u is observed, whose chattering effect on the signals is the most predominant, being LQR and MRAC the ones that cause this effect the most, generating a sudden and rapid change between the established saturation levels. Also, it can be noticed in MRAFC that the signals are smoother and more continuous in response to the step signal to which it was subjected, even in the interval $t = [84, 125]$, where a more unstable signal was expected and on the contrary responses with minimal and convergent oscillations were obtained.

B. *Follow-up*

The next step is to perform tests in the tracking phase, where now the input reference in the controllers is a user-defined trajectory. Therefore, for this purpose, it was decided to define a spiral trajectory generated with the algorithm established in section V, with a radius of $r = 2.5m$ and a depth of $h = 10m$.

This test is divided into three sections. First, to describe the behavior of the system when it is not subject to disturbances (an ideal environment). Second, when it is subject to an external force as a disturbance, the disturbance being a sinusoidal signal in the form of a wave with a height of $40cm$. And finally an analysis when it is subjected to constant noise.

1) Ideal conditions scenario: On the left side of Fig. 3 we have the position vector, where it is observed that the LQR signals control the system until time $t = 30s$, and then start a stage of instability. As could be seen in the previous section, when the controller moves away from its equilibrium state for which it was designed, it begins to generate instability. On the contrary, the MRAC and MRAFC controllers remain stable until the end of the travel.

On the right side of Fig. 3 the orientation vector is shown, where it is observed that the LQR begins a stage of instability from time $t = 30s$ in *roll*, where we can notice that at the end of the path the AUV converges again to the trajectory, this is because it approaches the original equilibrium point. In addition, it is noted that the variable *pitch* generates a steady-state tracking error in MRAFC mainly due to the linearization process of the nonlinear model, which can be attenuated by adding a PID controller.

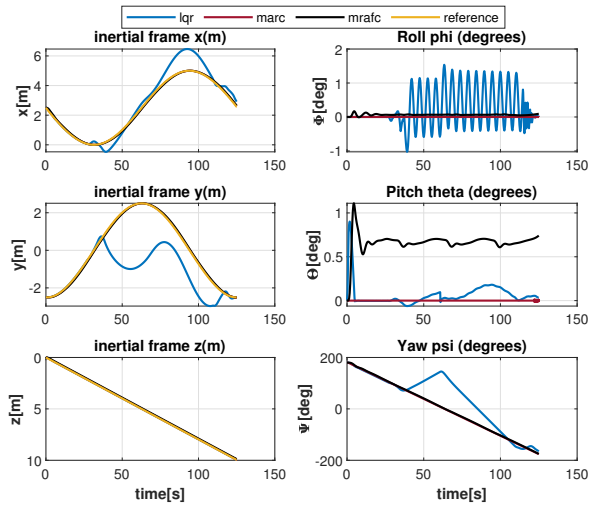

Fig. 3. Time response of the state vector η showing the dynamics of the AUV when traveling the spiral trajectory in the ideal conditions scenario. A convergent trajectory is observed for the MRAC and MRAFC controllers, while the LQR controller presents instability from time $t = 35$.

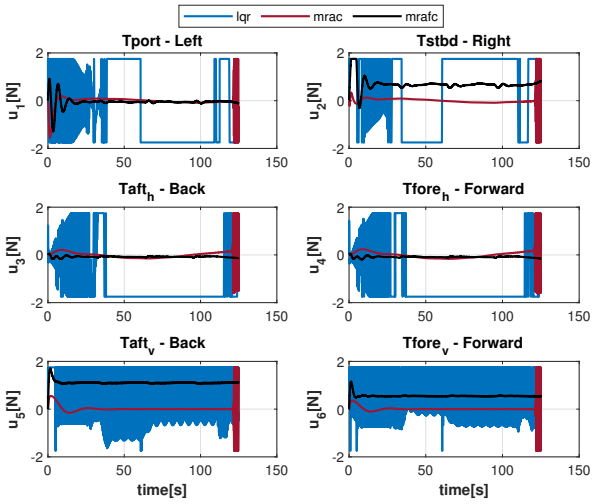

Fig. 4. Time response of the output vector u during the spiral trajectory in the ideal conditions scenario. Converging signals are observed throughout the entire trajectory when using the MRAFC controller, while in the MRAC controller a chattering effect is observed in the final part of the trajectory without causing instability in the AUV. On the contrary, total instability is observed when using the LQR controller.

The output vector u is shown in Fig. 4, with the chattering effect in LQR, while in MRAC it only presents this effect at the end of the path. In contrast, the response in MRAFC is smooth and continuous, presenting greater oscillation in the signals of the thrusters T_{port} and T_{stbd}.

An overview of the track is shown in Fig. 5. It can be noted that MRAC and MRAFC are the best at tracking the trajectory when the AUV is not subject to perturbations. Even under ideal conditions, the controllers must overcome the problem of the AUV's dynamic complexity and smoothly transition between linear subsystems, considering that they must generate a continuous control law without causing damage to the thrusters.

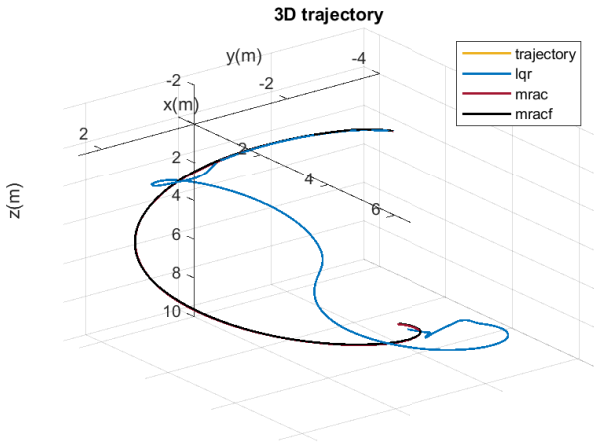

Fig. 5. 3D graph of the AUV's spiral trajectory under an ideal conditions scenario which does not present external disturbances or readings altered by inherent noise from the environment.

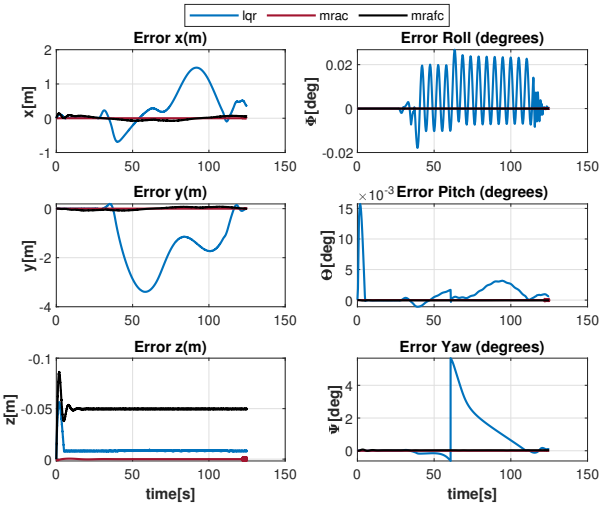

Fig. 6. Evolution over time of the tracking errors of the variable η. Highlighting the largest error in the LQR controller because during the trajectory the AUV moves away from the equilibrium point of the origin causing instability in the system.

Fig. 6 shows the evolution of errors in the variable η, observing a greater error in LQR due to the instability of the AUV. This is also confirmed by Table I, which gathers information on the ERMS performance indices of the controllers.

Furthermore, it can be verified that the lowest index is obtained by MRAC, followed by MRAFC and LQR. With this, the following sequence $MRAC > MRAFC > LQR$ can be obtained.

2) External Disturbance Scenario: In this test, a disturbance was designed to simulate a wave of height of 40cm based on the equation $\tau_{ext} = f\cos(\omega t)$. Saturated in the interval $t = [10, 20]$ to generate only one impulse. Considering that this disturbance is in the optimal working range for the controllers, it was decided to choose the beginning of the path which is closest to the initial equilibrium state and in this way

TABLE I
VARIABLE RMS ERROR η IN IDEAL CONDITIONS SCENARIO

	LQR	MRAC	MRAFC
x	0.6112	0.2494×10^{-3}	0.0654
y	1.6412	0.1624×10^{-3}	0.0625
z	0.0115	0.2831×10^{-3}	0.0793
ϕ	0.0104	0.0062×10^{-3}	0.0012
θ	0.0025	0.0205×10^{-3}	0.0118
ψ	1.5238	0.0745×10^{-3}	0.0396

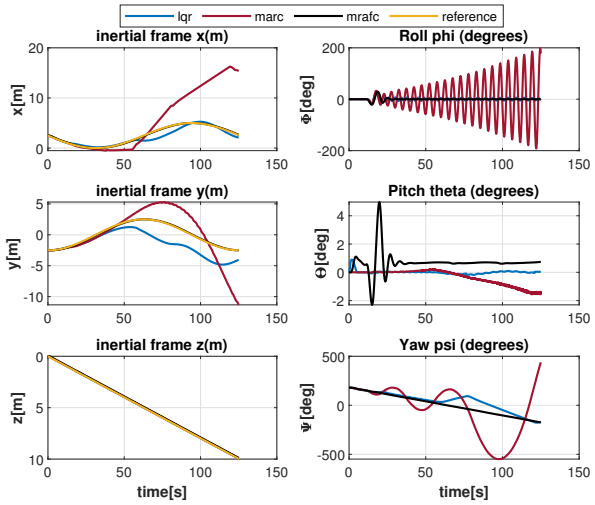

Fig. 7. Time response of the state vector η showing the dynamics of the AUV when traveling the spiral trajectory in the external disturbance scenario. Observing a convergent path only in the MRAFC controller, however now instability can be observed in the MARC and LQR controllers exactly after applying the external perturbation at time $t = 10$.

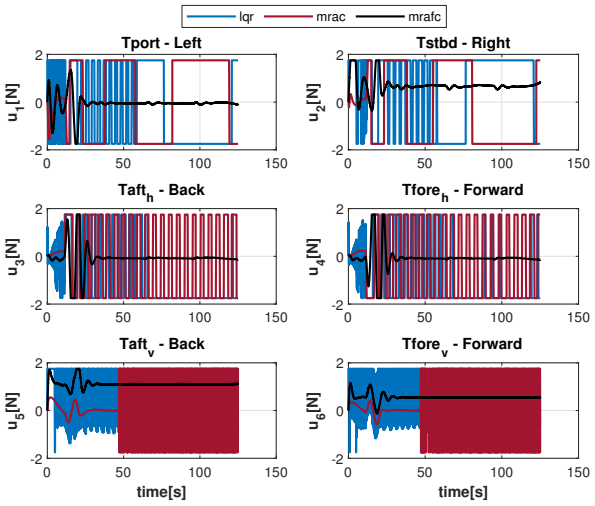

Fig. 8. Time response of the output vector u during the spiral path in the external perturbation scenario. Observing convergent signals only when using the MRAFC controller, while in the MRAC and LQR controllers the signals oscillate between saturation values causing again the chattering effect generating the instability.

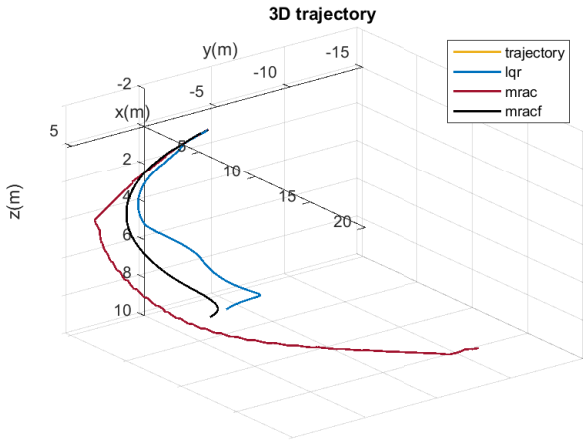

Fig. 9. 3D graph of the AUV spiral path under an external perturbation scenario which represents an environment exposed to 40cm high waves.

can correctly affect the LQR controller.

The left side of Fig. 7 shows the response of the position vector to a perturbation, where we can observe that the only controller capable of following the trajectory is MRAFC. Furthermore, the variables x and y of LQR and MRAC are unstable after the start of the perturbation, while z manages to converge to its reference trajectory. On the right side of Fig. 7 the orientation vector is shown, where the variables *roll* and *yaw* of MRAC are the most unstable, reaching angles of 200^o in *roll* and 500^o in *yaw*, while the variable *pitch* increases slowly with a maximum peak at the time of the perturbation of 4^o.

Fig. 8 shows the response of the vector u to a disturbance, observing an immediate response by raising the signal to the maximum to control the system. However, in LQR and MRAC this action is not enough, so they end up producing the chattering effect. While in MRAFC you can better appreciate the way of controlling and stabilizing where their signals converge, being smooth and continuous capable of being applied to the thrusters without causing future damage.

In Fig. 9, it is observed that the effect of the disturbance generates greater instability in the MRAC controller, however the LQR controller also suffers from instability, losing the course of the trajectory. On the contrary, the MRAFC controller converges to the desired trajectory. In Fig. 10 the evolution of the tracking error can be observed, confirming what was previously indicated, visualizing sinusoidal oscillations or simply divergences in the variables. In addition, to quantitatively support the results obtained, Table II is shown, whose data are obtained based on the ERMS performance indicator, identifying a greater error in MRAC and a smaller error in MRAFC. Obtaining a new order based on performance, such that $MRAFC > LQR > MRAC$.

As a final part of the scenario, the AUV stability limits were evaluated. Therefore, considering the previous results of the LQR and MRAC controllers, new perturbation limits were established only for the MRAFC controller, $\tau_{ext} = 1.0m$ and $\tau_{ext} = 1.2m$, whose results are shown in Fig. 11. From

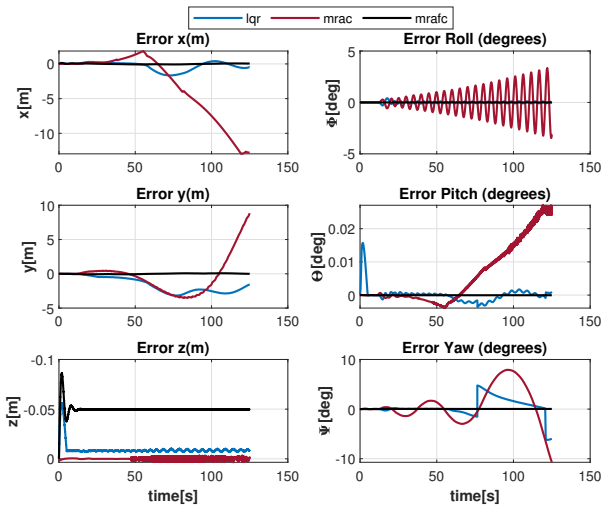

Fig. 10. Evolution over time of the tracking errors of the variable η. Considering that the 40cm high perturbation now causes instability in two controllers MRAC and LQR. Observing that the largest error is generated by the MRAC controller.

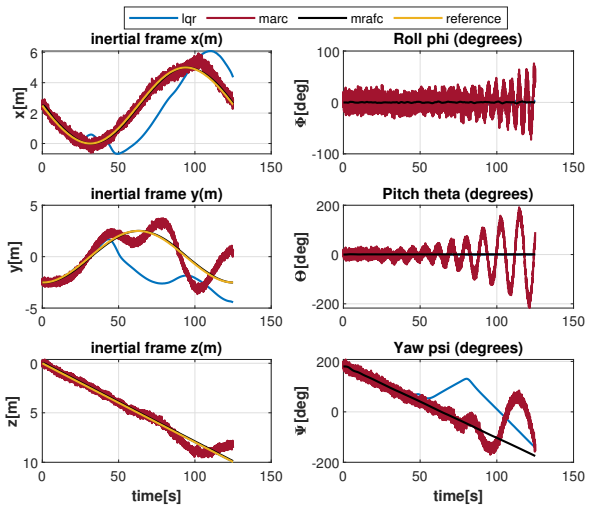

Fig. 12. Time response of the state vector η showing the dynamics of the AUV when traveling the spiral path in the noise scenario. A convergent path can be observed only in the MRAFC controllers, while the MARC and LQR controllers show instability again.

TABLE II
VARIABLE RMS ERROR η IN A DISTURBED SCENARIO

	LQR	MRAC	MRAFC
x	0.6822	5.4224	0.0654
y	1.9137	2.6114	0.0636
z	0.0115	0.0012	0.0793
ϕ	0.0906	1.2548	0.0866
θ	0.0024	0.0108	0.0117
ψ	1.8175	3.7446	0.0403

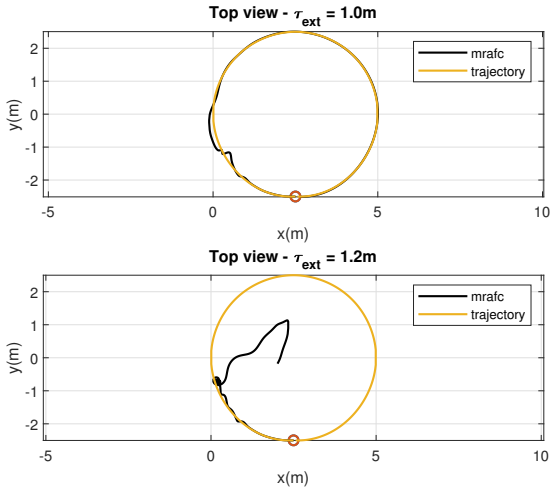

Fig. 11. Top view of the AUV in the external disturbance scenario. The upper graph shows temporal instability of the AUV for the value of $\tau_{ext} = 1.0m$, while the lower graph shows total instability for the value of $\tau_{ext} = 1.2m$

which we can observe that for a perturbation of $1.0m$ the AUV slightly leaves the trajectory but can recover the course and complete the route, while if the perturbation increases to $1.2m$ the system becomes unstable.

3) Noise scenario: In this section, the response of the AUV when it is subjected to a noisy environment. First, it was decided to generate the noise using the equation $noise = k{*}randn(n, 1)$, where the function *randn()* generates random numbers with a normal distribution and the variable k acts as the amplitude of the noise signal.

On the left side of Fig. 12 is the position vector, observing that the MRAC is more affected by noise generating the instability of the AUV. While LQR and MRAFC generate smooth and continuous signals, but only MRAFC manages to converge on the trajectory. Then, on the right side of Fig. 12 is the orientation vector, observing oscillating signals in MRAC reaching angles of 200^o in ϕ , 400^o in θ and -400^o in ψ. On the contrary, the signals generated by MRAFC converge asymptotically.

In Fig. 13, we can see the importance of the control signals generated in the thrusters for this effect to be shown in the state vector. That is, all the noise is cancelled in the orientation and position signals because the thrusters act in such a way that they generate stability in the AUV system. This can be observed in the MRAFC controller signals which are now not smooth and continuous but remain stable over time, and have minimal oscillation so it can be expected that it will not have negative effects on the useful life of the thrusters.

In Fig. 14, we notice that LQR and MRAC controllers are unstable, while MRAFC converges. However, we notice that the MRAC controller's trajectory absorbs all the noise effect, unlike the optimal control-based LQR and MRAFC controllers, whose trajectory signal is smooth. This is also reflected in the evolution of the tracking errors as shown in Fig. 15. Therefore, to quantitatively support the results, we have the information of the performance indices in Table III.

The new performance order for when the system is exposed to noise is given as $MRAFC > LQR > MRAC$.

The previous results were done using a value of $k = 0.15$, so to evaluate the limits of the MRAFC controller new values

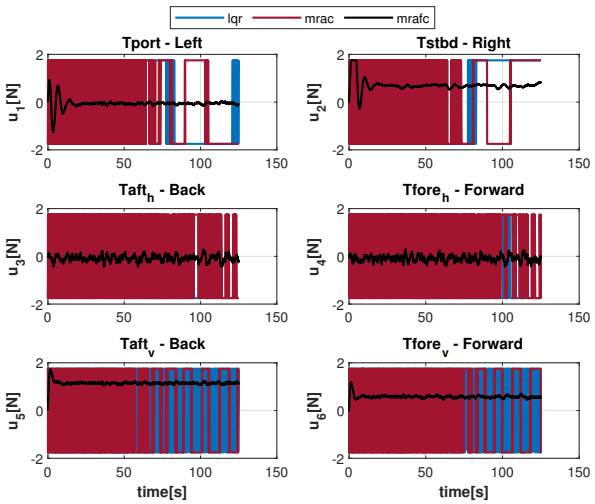

Fig. 13. Time response of the output vector u during the spiral path in the noise scenario. Highlighting the signal of the MRAFC controller which seems to have absorbed all the noise in order to stabilize the state vector of the AUV. While the MRAC and LQR controllers oscillate between saturation values.

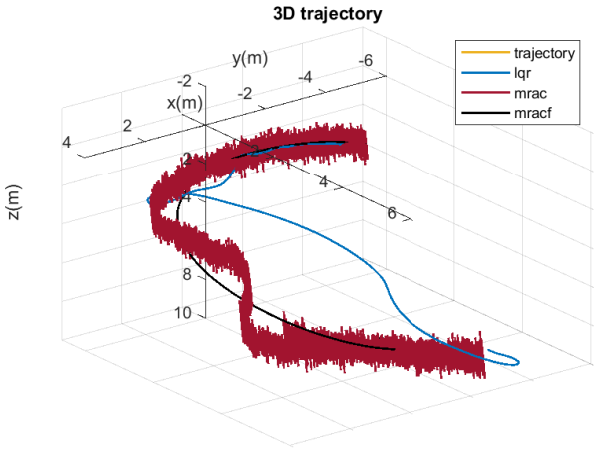

Fig. 14. 3D graph of the AUV's spiral path under a noise scenario representing a natural environment in the ocean.

TABLE III
VARIABLE RMS ERROR η IN NOISE SCENARIO

	LQR	MRAC	MRAFC
x	2.4640	2.1738	0.0662
y	1.8176	1.5721	0.0632
z	0.0120	0.3454	0.0817
ϕ	0.0364	0.7798	0.0101
θ	0.0052	1.5810	0.0121
ψ	2.0196	2.0267	0.0399

are considered, $k = 0.7$ and $k = 1.0$, whose results are shown in Fig. 16. Then, from the graph at the top corresponding to $k = 0.7$ we can observe that the AUV has sections where it moves away from the path caused by the increase in the noise amplitude to 70%, while if we consider the total amplitude obtained from the function *randn()* the system

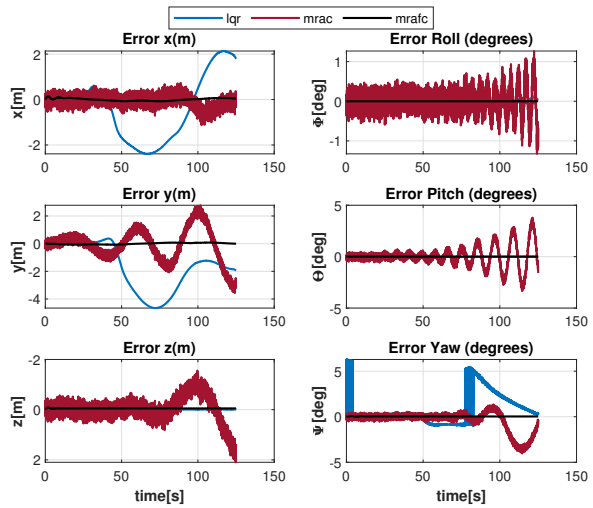

Fig. 15. Evolution over time of the tracking errors of the variable η. Highlighting the largest error in the LQR controller because during the trajectory the AUV moves away from the equilibrium point of the origin causing instability in the system.

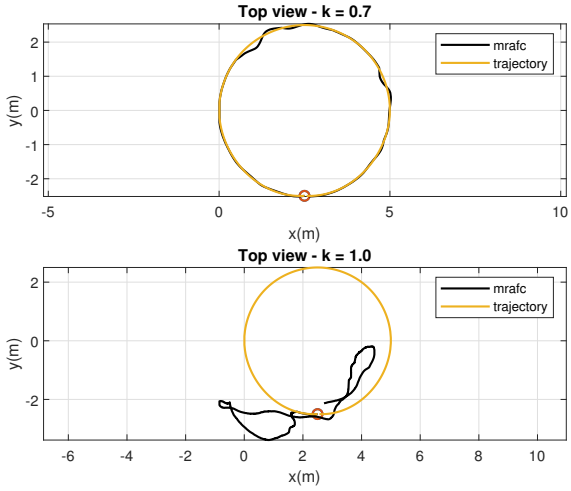

Fig. 16. Top view of the AUV in the noise scenario. The top graph shows the partial instability of the AUV when $k = 0.7$, while the bottom graph shows the total instability for the value of $k = 1.0$

becomes unstable.

VI. CONCLUDING REMARKS

In this research work, a robust MRAFC controller applied to a 6DOF AUV was designed to follow specific trajectories. A mathematical model was developed for the nonlinear AUV system, considering uncertain system parameters and the dynamic complexity of the ocean. Also, an MRAFC controller based on the Takagi-Sugeno MIMO type technique was developed, which adjusts the parameters of the control law based on the nonlinear Lyapunov control theory and numerical optimization calculation of LMIs, which ensure the desired navigation route. In addition, a comparative analysis was carried out between the MRAFC controller and conventional controllers such as LQR and MARC, using quantitative tables

of performance indices, resulting in the MRAFC controller being superior in the presence of disturbances and noise. Therefore, it is concluded from the results of this simulation that the MRAC controller is able to converge, follow the desired trajectory and establish the minimum tracking error under adverse conditions. Therefore, the next step will be to implement the MRAFC controller in a underwater robot implemented at the Advanced Control Laboratory of the PUCP.

ACKNOWLEDGMENTS

This work was supported by the Programa Nacional de Investigación Científica y Estudios Avanzados (PROCIENCIA) through the Convention: Proyectos de Desarrollo Tecnológico 2024-02 de PROCIENCIA-Consejo Nacional de Ciencia, Tecnología e Innovación (CONCYTEC) under Contract PE501086500-2024.

REFERENCES

[1] BBC N.M., 2023. [Online]. Available: https://www.bbc.com/mundo/articles/c16epene12jo.

[2] Gálvez, A, "Conservación del océano y las áreas marinas protegidas del Perú: alcances, legislación y retos. Lima: Sociedad Peruana de Derecho Ambiental," *SPDA*, 2022.

[3] Neil D. Burgess and Hilary Allison and Yara Shennan-Farpón and Ellen Shepherd, "El estado de la biodiversidad en America latina y el Caribe," *United Nations Environment Programme (UNEP)*, 2016.

[4] K. Mondal, Tanumoy Banerjee, Aniruddha Panja, " Autonomous Underwater Vehicles: Recent Developments and Future Prospects," *International Journal for Research in Applied Science and Engineering Technology (IJRASET)*, 2019. DOI:10.22214/ijraset.2019.11036.

[5] M. Balcazar, Gustavo Pérez-Zuñiga and Francisco Cuellar, "Design and Simulation of a Model Predictive Control System Navigation of a Drone in Confined Spaces," *International Conference on Artificial Intelligence, Computer, Data Sciences and Applications (ACDSA)*, 2024. DOI:10.1109/ISIE.2011.5984510.

[6] F. Hidalgo and Jose Mendoza and Francisco Cuéllar, "ROV-based acquisition system for water quality measuring," *OCEANS - MTS/IEEE Washington*, 2015. DOI:10.23919/OCEANS.2015.7404435.

[7] G. Antonelli, "Underwater Robots," *Springer Tracts in Advanced Robotics*, Vol. 96, 2014.

[8] L. Fenco,Gustavo Pérez-Zuñiga, Diego Quiroz and Francisco Cuellar, "Model Reference Adaptive Fuzzy Controller of a 6DOF Autonomous Underwater Vehicle," *IEEE-OCEANS: San Diego-Porto*, 2021. DOI:10.23919/OCEANS44145.2021.9706083.

[9] P. Van Tuan, "Maneuvering Algorithms of a Small-sized Underwater Robot," *IEEE Conference of Russian Young Researchers in Electrical and Electronic Engineering (EIConRus)*, IEEE, 2020. DOI:10.1109/EIConRus49466.2020.9039167.

[10] J. Igual Bañó, " Diseño e implementación de un algoritmo de control avanzado para la estabilización de un quadrotor basado en el autopiloto pixhawk y un sistema de posicionamiento rtk - gps," *Universitat Politècnica de València*, 2018.

[11] L. Priyadarsini, Dr. Shubhasri Kundu, Dr. Manoj Kumar Moharana, "Motion Control of AUV using IMC-PID Controller," *International Journal of Advanced Trends in Computer Science and Engineering*, 2020. DOI:10.30534/ijatcse/2020/171932020.

[12] J. Velagic, Nedim Osmic, Vedin Klovo and Halil Lacevi, "Design of LQR Controller for 3D Trajectory Tracking of Octocopter Unmanned Aerial Vehicle," *International Conference on Control, Decision and Information Technologies (CoDIT)*, 2022. DOI:10.1109/CoDIT55151.2022.9803884.

[13] H. Ventura–Hinostroza and Arturo Rojas–Moreno, "Real–Time Model Reference Adaptive Control of a 3DOF Robot Arm," *IEEE XXVI International Conference on Electronics, Electrical Engineering and Computing*, 2019. DOI:10.1109/INTERCON.2019.8853622.

[14] N. Nayak, Pranati Das and Soumya Ranjan Das, "Heading plane Control of an Autonomous Underwater Vehicle: A novel Fuzzy and Model Reference Adaptive Control Approach," *Third International Conference on Advances in Electronics, Computers and Communications (ICAECC)*, 2020. DOI:10.1109/ICAECC50550.2020.9339495.

[15] Z. Liu, Xinliang Wang, Xiawei Guan, Zhesong Ma, Pingpeng Tang, Chao Zheng, "Precise Docking Control of AUV Based on Neural Network Adaptive Controller," *IEEE 8th International Conference on Underwater System Technology: Theory and Applications (USYS)*, 2018. DOI:10.1109/USYS.2018.8778910.

[16] A. Huaman Loayza and Gustavo Pérez Zuñiga, "Design of a fuzzy sliding mode controller for the autonomous path-following of a quadrotor," *IEEE Latin America Transactions*, pp.962-971, 2019. DOI: 10.1109/TLA.2019.8896819.

[17] W. Zhang, Wenhua Wu, Zixuan Li, Xue Du and Zheping Yan, " Three-Dimensional Trajectory Tracking of AUV Based on Nonsingular Terminal Sliding Mode and Active Disturbance Rejection Decoupling Control," *Journal of Marine Science and Engineering*, 2023. DOI:10.3390/jmse11050959.

[18] Y. Valeriano, A. Fernández, L. Hernández and P. J. Prieto, "Yaw Controller in Sliding Mode for Underwater Autonomous Vehicle," *IEEE LATIN AMERICA TRANSACTIONS*, 2016. DOI: 10.1109/TLA.2016.7459601.

[19] J. Yuan, Hongjian Wang, Honghan Zhang, Changjian Lin, Dan Yu and Chengfeng Li, "AUV Obstacle Avoidance Planning Based on Deep Reinforcement Learning," *Journal of Marine Science and Engineering*, 2021. DOI:10.3390/jmse9111166.

[20] T. I. Fossen, "Handbook of marine craft hydrodynamics and motion control," *John Wiley and Sons Ltd. Published*, First Edition, 2011.

[21] Manhar R. Dhanak and Nikolaos I. Xiros, "Ocean Engineering," *Springer Handbook*, 2016.

[22] A. Sahoo, Santosha K. Dwivedy and P. S. Robi, "Adaptive Fuzzy PID Controller for A Compact Autonomous Underwater Vehicle," *Global Oceans*,2020. DOI:10.1109/IEEECONF38699.2020.9389483.

[23] Xin-Yu Liu, Yi-Ping Li, Shu-Xue Yan, Xi-Sheng Feng, "Adaptive attitude controller design of autonomous underwater vehicle focus on decoupling," *IEEE Underwater Technology (UT)*,2017. DOI:10.1109/UT.2017.7890325.

[24] G. Lai, Yun Zhang, Zhi Liu, Junwei Wang and C. L. Philip Chen, "Direct Adaptive Fuzzy Control Scheme With Guaranteed Tracking Performances For Uncertain Canonical Nonlinear Systems," *IEEE Transactions on Fuzzy Systems*, vol. 30, pp. 818–829, 2022. DOI:10.1109/TFUZZ.2021.3049902.

[25] K. Lu, Zhi Liu, C.L.Philip Chen, Yaonan Wang and Yun Zhang, "Inverse Optimal Design of Direct Adaptive Fuzzy Controllers for Uncertain Nonlinear Systems," *IEEE Transactions on Fuzzy Systems*, vol. 30, pp. 1669–1682, 2022. DOI:10.1109/TFUZZ.2021.3064678.

Lugui Paolo Fenco Bravo graduated in Electronic Engineering from the Universidad Nacional Pedro Ruiz Gallo, Lambayeque, Peru in 2015. He received the master degree in Control and Automation Engineering from Pontifical Catholic University of Peru (PUCP), Lima, Peru in 2024. His current research interests include nonlinear control systems, fuzzy systems, optimal control and trajectory analysis in autonomous underwater vehicles.

Gustavo Pérez Zuñiga received the Ph.D. degree in Control Engineering from the Federal University of Toulouse Midi- Pyrénées (UFTMP), Toulouse, France in 2017. He received the master degree in Control and Automation Engineering from Pontifical Catholic University of Peru (PUCP), Lima, Peru in 2008. Currently, he is Featured Researcher and Full Professor in the Engineering Department of the the Pontifical Catholic University of Peru. His current research interests include advanced control and fault diagnosis for large-scale complex and robotics systems with special focus on data-based and model-based methods. Dr. Pérez-Zuñiga is a member of the Safeprocess Technical Committee (https://tc.ifac-control.org/6/4) of the International Federation of Automatic Control.